

# Optical and Infrared Photometry of the Micro-quasar GRO J1655-40 in Quiescence

Jenny Greene, Charles D. Bailyn

*Astronomy Department, Yale University, PO Box 208101, New Haven CT, 06520-8101, USA*

jenny.greene@aya.yale.edu; bailyn@astro.yale.edu

Jerome A. Orosz

*Astronomical Institute, Utrecht University, PO Box 80000, 3508 TA Utrecht, The Netherlands*

J.A.Orosz@astro.uu.nl

## ABSTRACT

We present *BVIJK* photometry of the black-hole candidate GRO J1655-40 in full quiescence. We report a refined orbital period of  $2.62191 \pm 0.00020$  days. The light curves are dominated by ellipsoidal variations from the secondary star. We model the light curves with an upgraded code which includes a more accurate treatment of limb darkening. Previous models containing a large cool disk are ruled out, and indeed our data can be fit with a pure ellipsoidal light curve without any disk contribution. In general agreement with previous results, we derive a confidence region of the correlated quantities inclination and mass ratio, centered on an inclination of  $70.2 \pm 1.9^\circ$  and mass ratio of  $2.6 \pm 0.3$ , resulting in a primary mass  $M_1 = 6.3 \pm 0.5 M_\odot$  (all 95% confidence). The complex limits and errors on these values, and on the possible disk contribution to the light curve, are discussed.

*Subject headings:* black holes, X-ray sources, binary stars.

## 1. Introduction

The Soft X-ray Transients (SXT) are a sub-class of accreting low-mass binary systems consisting of a neutron star or black hole primary, accretion disk, and Roche lobe filling secondary star. Instabilities in mass accretion cause these sources to undergo episodic outbursts. The X-ray emission during outburst indicates the existence of an accreting compact object. During outburst, the accretion flow contributes nearly all the optical flux. In quiescence, on the other hand, the X-ray luminosity is very low, and the optical light is dominated by the contribution of the secondary star. At this time the orbital characteristics of the SXT's may be studied in some detail (van Paradijs and McClintock 1995). In particular, the mass function can be measured, which provides

a lower limit to the mass of the compact object. Further information about the mass ratio (from line broadening) and inclination (from ellipsoidal variability) can be used to determine the mass of the compact object (Bailyn et al. 1998, and references therein) which in many cases is above the  $3 M_{\odot}$  upper limit of the mass of a neutron star (Chitre and Hartle 1976).

While this procedure has been carried out successfully for several systems (see references in Bailyn et al. 1998), the modeling of ellipsoidal variations can be complicated by various other contributions to the observed light curves, in particular contributions from the accreting material. The accretion flow typically contributes both a constant flux offset and random flickering. The constant flux contribution of the disk decreases the observed amplitude of the ellipsoidal variations, and is thus degenerate with the inclination to first order (there are potentially observable shape differences). In systems for which the disk contribution is significant, not only is the amplitude of the variations decreased, but the aperiodic flickering may result in changes in the light curve from measurement to measurement, complicating the process of accurately modeling the light curve. One proposed method to minimize the disk contribution is the use of infrared light curves. For example, Shahbaz, Naylor, & Charles (1994) suggest that the disk contribution to the light curves of A0620–00 are minimized in the infrared. They have directly measured the disk contribution in the  $K$ -band spectroscopically, and find it to be less than 27%, smaller than in the optical (Shahbaz, Bandyopadhyay, & Charles 1999a).

Models used to fit the ellipsoidal variations of SXT’s in quiescence have traditionally assumed accretion flow in the form of a geometrically thin, optically thick disk (e.g. Orosz and Bailyn 1997, hereafter OB97; van der Hooft et al. 1998). The standard thin  $\alpha$ -disk model corresponds to one allowed solution to the hydrodynamic equations which describe differentially rotating gas flows (Shakura and Sunyaev 1973; Frank, King & Raine 1992). The  $\alpha$ -disk model has been successfully used to model the outburst cycle of cataclysmic variables (e.g. Cannizzo 1993). However, recent findings have called into question the application of standard thin disk to model SXT systems. In particular, Narayan and collaborators have suggested that the accretion flow in quiescence consists of an outer disk and an optically thin advection dominated flow closer to the compact object (Narayan, McClintock, & Yi 1996).

The SXT GRO J1655–40 (Nova Sco 1994) was discovered on July 7 1994 with the Burst and Transient Source Experiment aboard the *Compton Gamma Ray Observatory* (Zhang et al. 1994). Because GRO J1655–40 has a relatively luminous F star secondary the quiescent light curves are dominated by star light to an unusually large extent. As a result, an unusually precise fit of the orbital parameters is possible. OB97 report values of  $P_{orb} = 2.62157 \pm 0.00015$  days,  $f(M) = 3.24 \pm 0.09 M_{\odot}$ ,  $i = 69.50 \pm 0.08^{\circ}$ , and  $Q = 2.99 \pm 0.08$  (where  $Q$  is taken to be  $M_1/M_2$ ) resulting in a primary mass of  $7.09 \pm 0.22 M_{\odot}$ . van der Hooft et al. (1998) derive a refined  $P_{orb} = 2.62168 \pm 0.00014$  days from photometric and spectroscopic quiescent data taken before the April 1996 outburst. They use  $f(M) = 3.16 \pm 0.15$  (Bailyn et al. 1995b), and report a range of secondary mass  $1.60 \lesssim M_2 \lesssim 3.10 M_{\odot}$  and  $i$  of  $63.7 \lesssim i \lesssim 70.7^{\circ}$ , corresponding to a primary mass range of  $6.29 - 7.60 M_{\odot}$ . Shahbaz et al. (1999b) obtained improved spectroscopy, and report  $f(M) =$

$2.73 \pm 0.09 M_{\odot}$  and a range of  $q = M_2/M_1$  of  $0.337 - 0.436$ . They derive a primary mass of  $5.5 - 7.9 M_{\odot}$ . Using Keck spectroscopy, Israelian et al. (1999) found a rotational velocity for the secondary star of  $v_{\text{rot}} \sin i = 93 \pm 3 \text{ km s}^{-1}$ , which implies a mass ratio of  $Q = 2.48 \pm 0.16$  (assuming synchronous rotation and using the Shahbaz et al. mass function). No infrared data have been available to date.

We have obtained *BVIJK* light curves in order to explore the nature of the quiescent accretion flow and to further constrain the orbital parameters of the system. In §2 we present the data and reduction techniques. In §3 we discuss the values and limits on the orbital parameters and disk contribution. Our results are summarized in §4.

## 2. Observations and Reductions

Photometry of the source was obtained from 1999 July through October with ANDICAM<sup>1</sup> on the 1.0 meter Yale telescope at CTIO, operated by the YALO Consortium (Bailyn et al. 1999). ANDICAM is capable of observing at an optical and an infrared wavelength simultaneously. The source was observed in the Johnson *BVI* filters with a Loral  $2048 \times 2048$  CCD and the *JK* infrared filters with a Rockwell  $1024 \times 1024$  HgCdTe HAWAII Array. The infrared channel of ANDICAM allows for a dither pattern of up to seven positions. An observing sequence consisted of a single 720 second exposure in *B* simultaneously with seven dithered 100 second exposures in *J*, followed by a single 360 second exposure in *V* simultaneously with seven dithered 45 second exposures in *K*, followed by a single 180 second exposure in *I* simultaneously with 4 dithered 45 second exposures in *K*. We typically performed one observing sequence per night between 1999 July 7 and 1999 October 30 (HJD 2,451,376–2,451,481).

The optical images were bias and flat-field corrected using standard IRAF routines. Sky corrections for the infrared frames were constructed by median-combining all frames from a given night of the same filter. This sky field was subtracted from each image in the set. A flat-field was constructed by taking the difference between a dome flat taken with dome-lights on, and one taken with dome-lights off. Finally, the images from each set were co-added.

The program DAOPHOT II (Stetson 1987) within IRAF was used to remove near neighbors of the program object and all comparison stars. Aperture photometry was then performed on the cleaned images. The magnitudes of at least 30 nearby stable stars were combined to form a comparison sequence for the differential photometry. Time-series were constructed in each filter (see Figure 1). In order to estimate the accuracy of our photometry, we extracted  $\sim 5$  stable comparison stars which span the magnitude range of the source. We measured the scatter of each comparison star about its mean, and use the average rms of all the comparison stars as our estimate for the scatter in the program object photometry. We find the average rms of these comparison

---

<sup>1</sup><http://www.astronomy.ohio-state.edu/~depoj/research/instrumentation/andicam/andicam.html>

stars to be 0.017 mag in the  $B$  and  $V$  filters, 0.014 mag in the  $I$ , 0.023 mag in  $J$  and 0.032 mag in  $K$ .

Our  $BVIJK$  light curves are presented in Figure 1 phased on our current best period of  $2.62191 \pm 0.00020$  days ( $1 \sigma$  error). They are plotted with a stable comparison star of similar magnitude in order to demonstrate the scatter in the photometry. The data have been phased following the convention of OB97 in which phase 0 corresponds to the closest approach of the secondary star to the observer. The light curves are dominated by ellipsoidal variations, demonstrating two minima per orbit. We observe a deeper minimum at phase 0.5, which is explained by increased gravity darkening near the inner Lagrangian point. The optical light curves are quantitatively indistinguishable from those reported by OB97 and van der Hooft et al. (1998). This result confirms that the data obtained in March 1996 was truly in full quiescence, and demonstrates that the source has returned to the same state after the outburst which began in April 1996 (Orosz et al. 1997). The  $JK$  light curves are similar in shape to the optical curves. The increased scatter in the  $K$  band is consistent with the increased scatter in the comparison stars, and does not require intrinsic source variability.

We find a deviant high point corresponding to  $\text{HJD} \sim 2,451,476.5$ . In all cases but the  $V$  band, data from this date lie significantly above the rest of the light curve, possibly due to a flare or a hot spot. This is unexpected, given the small contribution of the accretion flow. We removed this point for purposes of model fitting.

In order to find an improved value for the orbital period we combined our data with the OB97 quiescent data (Figure 2). We were unable to phase the combined data set on the OB97 spectroscopic period of  $2.62157 \pm 0.00015$  days. However, OB97 used both quiescent and outburst radial velocity data to calculate this period. As pointed out by Shahbaz et al. (1999b), X-ray heating of the secondary star can cause the ‘effective center’ of the secondary to shift, making a sinusoidal fit inadequate. The OB97 period is therefore suspect. Using our data set in conjunction with only the photometric data set of OB97, we found a preferred photometric period of  $2.62191 \pm 0.00020$  days from the Phase Dispersion Minimization (Stellingwerf 1978) package in IRAF. The Lomb-Scargle (Press and Rybicki 1989) and Clean (Roberts, Lehár, and Dreher 1987) algorithms within the Period package<sup>2</sup> gave similar results. This period is consistent with the published photometric period of  $2.62168 \pm 0.00014$  days of van der Hooft et al. (1998).

### 3. Discussion

Our primary purpose in measuring multiwavelength quiescent light curves of SXT’s is to constrain the disk contribution in quiescence. This is not only interesting in itself but provides a crucial input into the determination of inclination and therefore to the determination of the mass of the

---

<sup>2</sup><http://www.starlink.rl.ac.uk/star/docs/sun167.htx/sun167.htmlstardoccontents>

primary as well as other binary system parameters.

Past work on GRO J1655–40 has consistently found a model with an extended cool disk to best fit the data. In particular, the depth of the minimum at phase 0.5 (OB97 convention) in the  $B$  light curve could not be fit without a grazing eclipse of the star by the disk. Since the size of such an eclipse is a very strong function of inclination, very tight limits on  $i$  were derived (OB97, van der Hooft et al. 1998). At the same time, the small relative contribution of light from the disk in the optical wavebands required a very cool outer disk. The current work has improved on previous studies in two significant ways. We use an improved modeling code which uses model atmosphere tables to compute local intensities, providing significantly improved limb darkening calculations. In addition we have obtained infrared data, allowing us to better constrain the contribution of the outer parts of the disk, which are cooler than the star.

We used the recently developed ELC code (Orosz & Hauschildt 2000, hereafter OH2000) to model the light curves. This code, which is loosely based on the code described in OB97, uses model atmosphere specific intensities rather than specific intensities computed using black bodies and a one- or two-parameter limb darkening law. For the present problem we used the NEXTGEN grid for cool giants (Hauschildt et al. 1999). The NEXTGEN models are the most comprehensive and detailed models available for cool stars. The model atmospheres are computed using spherical geometry, rather than the usual plane-parallel approximation. OH2000 show that for low gravity stars ( $\log g \lesssim 3.5$ ) the limb darkening behavior of the extended spherical models deviates significantly from a simple linear law. Since the secondary star in GRO J1655-40 has a relatively low gravity ( $\log g \lesssim 3.5$  in general, and formally reaching zero at the  $L_1$  point itself) the consequences of the nonlinear limb darkening are likely to be important. In general, the NEXTGEN models predict a lower intensity near the limb of the star. The overall result is that in most cases the amplitude of the ellipsoidal light curve is *larger* when the NextGen intensities are used compared to the light curve computed using black body intensities (see OH2000 for a detailed discussion of this point). This effect is maximized in the bluest band passes, where a small downward shift in temperature makes the biggest decrease in flux. Note that it is precisely the  $B$  band lightcurve near phase 0.5 which OB97 suggest requires the partial eclipse.

Our primary conclusion based on modeling the new data with the new code is that the large, cool disk and partial eclipse advocated in our previous study (OB97) and that of van der Hooft et al. (1998) is no longer viable. Indeed, we find no evidence for *any* contribution from the accretion flow to the optical/IR lightcurves. In Figure 1 we have plotted our data with the large disk model (computed with the improved model atmosphere code) which provides the best fit to the OB97 data. While this model fits our optical data as well as it fits the OB97 data, it fails dramatically in the IR, where the large contribution from the cool disk dilutes the ellipsoidal light curves too much. In fact, a model with an eclipsing cool outer disk would require an outer disk temperature on the order of 100  $K$  as found by van der Hooft et al. (1998). We argue below that such a low outer disk temperature is physically implausible, due to the radiation field of the F–star companion. Alternatively, all bandpasses are well fit by a model with no disk contribution or eclipses (see Fig.

2). The two models (with or without disk) are statistically indistinguishable in terms of their fit to the  $B$  band at phase 0.5. There is still a small residual discrepancy, but it is similar in size for both models, in contrast with the results of OB97 who found that with their cruder modeling of limb darkening the partial eclipse model fit significantly better.

A large cool disk with an outer temperature of 100  $K$  also seems improbable given the proximity of an F-star companion. While it is beyond the scope of this paper to solve the detailed equations of gas dynamics and radiative transfer to determine the outer disk temperature, it seems reasonable to derive an approximate lower limit on this temperature due to the radiation field of the companion star. The ratio of flux from the companion star at the point of the disk nearest the  $L_1$  point to that at the surface of the star itself is approximately  $(R_{star}/D_{disk})^2$  where  $R_{star}$  is the effective radius of the secondary star calculated using the Eggleton approximation (Eggleton 1983) and  $D_{disk}$  is the closest distance between the center of the secondary star and the outer edge of the accretion disk. Thus the black-body temperature generated by the star’s radiation field when it impacts the outer edge of the (presumably optically thick) disk would be

$$T_{edge} = \sqrt{\frac{R_{star}}{D_{disk}}} \times T_{star}.$$

where  $T_{edge}$  is the temperature due to the radiation field of the star at that point and  $T_{star}$  is the mean surface temperature of the star. Since all the gas in the outermost regions of the disk originated on the secondary star and continues to be irradiated by the secondary at least some of the time as it orbits the primary,  $T_{edge}$  may provide a rough lower limit to  $T_{outer}$ . We emphasize that the actual value of  $T_{outer}$  depends on the temperature of the gas as it leaves the  $L_1$  point (which may be considerably cooler than the average temperature of the star), the gravitational potential energy gained by the gas as it falls toward the disk, and any density change or thermal energy transfer which may occur upon the impact of the gas with the accretion disk.

Figure 3 displays limits on the extent and outer temperature of the quiescent disk. The allowed region is bounded at low  $T_{outer}$  by  $T_{edge}$ . An upper limit on  $T_{outer}$  can be derived empirically by computing the limits on the disk contamination of the ellipsoidal lightcurves. We have done this by approximating the accretion flow as a black-body disk with a single temperature equal to that at the outer edge. This provides an appropriate limiting case, as any temperature rise toward the center of the disk will increase the total flux contribution of the disk resulting in more stringent limits. We model the disk flux contribution as a constant dilution factor to the ellipsoidal lightcurves, taking into account the system inclination and an assumed outer disk radius. The f-statistic is used to compare the resulting lightcurves with our data, and determine whether they are statistically different at the one and three  $\sigma$  level. Table 1 lists the allowed one and three  $\sigma$  disk dilution limits for each filter computed from the model fits. The curves shown in Figure 3 are derived from the  $V$  band data, which provided the tightest constraint on the allowed disk region. Note that the limits for the combined light curves are much more severe than for any one filter, both because there are many more data points involved and because any contribution from the disk would be maximized in one particular bandpass, and thus would have to be much lower in most of the others. Finally,

Figure 3 also shows the disk size at which partial eclipses of the star by the disk would occur. Note that this is a somewhat porous limit, since it varies with  $i$  and  $Q$ , but it demonstrates the qualitative effect of the lack of evidence for such eclipses.

Based on the arguments presented above, we adopted a model which consists only of ellipsoidal variations from the Roche-lobe filling secondary. Hence the only free parameters are the mass ratio  $Q$  and the inclination  $i$ . We adopted a spectral type of F6III (Shahbaz et al. 1999b), which corresponds to a mean secondary star temperature of  $T_{\text{eff}} = 6336$  K (Gray 1992). We had three basic binary system observables, namely the photometric light curves in the five filters, the radial velocity curve (Shahbaz et al. 1999b), and the measurement of the mean projected rotational velocity of the secondary star  $v_{\text{rot}} \sin i$  (Israelian et al. 1999). All of these observables were obtained when the source was in complete X-ray quiescence ( $L_x \leq 10^{-3} L_{\text{opt}}$ ). Thus the light curves and the velocity curve did not suffer any biases caused by X-ray heating. It is well known that tidal distortion of the secondary star can cause distortions in the line profiles from which the rotational velocity is measured, leading to a systematic error in  $v_{\text{rot}} \sin i$  (e.g. Kopal 1959; Marsh, Robinson, & Wood 1994; Shahbaz 1998; OH2000). However, the measurement of the rotational velocity was obtained at the photometric phase 0 (i.e. the closest approach of the F-star), which is the phase when the potential distortions to the line profiles are minimized. We computed numerical broadening kernels for phase 0 and compared them to the analytic kernel commonly used and found almost no systematic biases. We conclude that the Israelian et al. (1999) value of  $v_{\text{rot}} \sin i$  represents the true mean projected rotational velocity of the F-star.

Our fitting procedure makes use of all of the binary system observables and their uncertainties. We will analyze three different data sets together. First are the photometric light curves reported in this paper. There are a total of 227 observations in the five filters (48, 48, 47, 43 and 41 in B, V, I, J, and K respectively). The second data set is the radial velocity curve of Shahbaz et al. (1999), which has 29 points. Finally, the single measurement of  $v_{\text{rot}} \sin i = 93 \pm 3$  kms $^{-1}$  provided by Israelian et al. (1999) is our third data set. We seek a binary system model which best fits all three basic observables simultaneously, i.e. we minimize the total  $\chi^2$ :  $\chi_{\text{tot}}^2 = \chi_{\text{photo}}^2 + \chi_{\text{rmRV}}^2 + \chi_{\text{rot}}^2$ .

There is some ambiguity in assigning weights to the various observations when fitting several quantities simultaneously. In this case, we simply assigned equal weights to each of the three data sets. For the data sets to be weighted equally requires that the values of  $\chi^2$  associated with the best fit to each one be the same. A three-parameter sinusoid fit to the Shahbaz et al. (1999) radial velocities yields  $\chi_{\text{RV}}^2/\nu = 0.98$ . We therefore take the quoted uncertainties on each radial velocity measurement at face value. We also adopted the  $1\sigma$  uncertainty in  $v \sin i$  quoted by Israelian et al. (1999). In the case of our photometry, however, using the observational uncertainties derived from comparison stars resulted in  $\chi^2/\nu > 1$  for our best fits. Therefore we have arbitrarily increased the errors used for each point by a factor of 1.27, which yields  $\chi^2/\nu = 1$  for the best fits.

We then defined a grid of points in the  $Q$ - $i$  plane where  $2.0 \leq Q \leq 3.65$  in steps of 0.05 and  $66^\circ \leq i \leq 74.8^\circ$  in steps of  $0.2^\circ$ . At each point in this grid the orbital separation  $a$  was adjusted

to minimize the total  $\chi^2$ . The orbital separation is needed to convert the model velocity curve and rotational velocity into physical units, and is also needed for the computation of the light curve, since the model atmosphere intensities are tabulated as a function of the gravity in physical units.

Using this procedure, we find a minimum overall  $\chi_{\text{tot}}^2$  at  $Q = 2.6$  and  $i = 70.2^\circ$  (see Table 2). This point and  $\chi^2$  contours denoting the one and three  $\sigma$  confidence limits are shown in Figure 4. Combining the allowed regions in  $Q$  and  $i$  shown in Figure 4 with the Shahbaz et al. (1999b) mass function  $f(M)$ , we find the probability distribution for  $M_1$  shown in Figure 5. To obtain this curve we divided the  $Q - i$  plane into 50 confidence regions corresponding to the probability associated with  $\chi_{\text{tot}}^2$ . Then we selected equal numbers of  $Q, i$  pairs in each confidence region, and for each  $Q, i$  pair chose values of  $f(M)$  based on the Shahbaz et al. (1999b) value and error. A more detailed discussion of this procedure may be found in Orosz & Wade (1999). The probability density shown in Figure 5 is obtained by calculating an  $M_1$  for each point in the  $(Q, i, f(M))$  space, and summing the resulting values of  $M_1$  weighted by an appropriate likelihood. The likelihood  $L_{Qif}$  of each combination of  $Q, i$ , and  $f(M)$  is determined by

$$L_{Qif} = \exp[-\chi_{Qi}^2 - \chi_f^2]$$

where  $\chi_{Qi}^2$  is the reduced  $\chi^2$  determined for the relevant values of  $Q$  and  $i$  as described above, and  $\chi_f = (f - f_m)/\sigma_f$ , where  $f_m$  is the value of  $f(M)$  measured by Shahbaz et al. (1999b) and  $\sigma_f$  is their quoted error. The distribution shown in Figure 5 is then the normalized probability distribution created by summing all the values of  $M_1$  weighted by their likelihoods. We find a preferred  $M_1$  value of  $6.3 \pm 0.5 M_\odot$  (95% confidence). The peak of this distribution is lower than the result quoted in OB97 due to the lower value of  $f(M)$  determined by Shahbaz et al. (1999b), and the distribution is wider than the errors quoted by OB97 because the limits on the inclination are less stringent without the requirement for a partial eclipse.

#### 4. Summary

We present *BVIJK* quiescent light curves of the SXT GRO J1655–40. The shape of our light curves is consistent with that of previously published results, supporting the assumption that the source truly went into quiescence in 1996 before its most recent outburst. We report a refined photometric period of  $2.62191 \pm 0.00020$  days. We find that our best fit to the data at all wavelengths is provided by a model with no contribution from an accretion flow. For this fit we find a range in  $i$  and  $Q$  shown in Figure 4, which is consistent with, but somewhat wider than, previous findings. We also find a probability distribution of  $M_1$  shown in Figure 5 where  $M_1 = 6.3 \pm 0.5 M_\odot$  (95% confidence). We have placed limits on the temperature and physical size of any accretion disk component.

This research was supported by NSF grant AST–9730774. Construction of the ANDICAM was carried out by the Ohio State University astronomical instrumentation group and sponsored by the



NSF grant AST–9530619. We are grateful for conversations with Darren Depoy and Rick Pogge about the performance of the instrument, and with Nick Suntzeff about the calibration of the IR channel. David Gonzalez and Juan Espinoza provided their usual expert services as mountain-top observers, and Suzanne Tourtellotte managed the data processing with her usual aplomb. Shahbaz et al. (1999b) were kind enough to provide the RV data. We thank Elene Terry for development of the data processing software and Raj Jain for his software expertise and endless patience.

## REFERENCES

- Bailyn, C.D., Depoy, D., Agostinho, R., Mendez, R., Espinoza, J., & Gonzalez, D., 1999 AAS 195, 8706
- Bailyn, C.D., Orosz, J.A., McClintock, J.E., & Remillard, R.A., 1995, *Nature*, 378, 157
- Bailyn, C.D., Jain, R.K., Coppi, P., & Orosz, J.A., 1998, *ApJ*, 499, 367
- Cannizzo, J.K., 1993, in *Accretion Disks in Compact Stellar Systems*, ed. J. C. Wheeler (Singapore: World Scientific), 6
- Chitre, D.M., and Hartle, J.B., 1976, *ApJ*, 207, 592
- Eggleton, P.P., 1983, *ApJ*, 268, 368
- Frank, J., King, A., & Raine, D., 1992, *Accretion Power in Astrophysics*, Cambridge Astrophysics Series, (Cambridge: Cambridge University Press)
- Gray, D., 1992, *Observation and Analysis of Stellar Photospheres*, (Cambridge: Cambridge University Press)
- Hauschildt, P. H., Allard, F., Ferguson, J., Baron, E., & Alexander, D. R. *ApJ*, 525, 871
- Israelian G., Rebolo R., Basri G., Casares J., Martin E. L., 1999, *Nature*, 401, 142
- Kopal Z., 1959, *Close Binary Systems*. (New York: John Wiley & Son)
- Marsh T. R., Robinson E. L., Wood J. H., 1994, *MNRAS*, 266, 137
- Narayan, R., McClintock, J.E., Yi, I., 1996, *ApJ*, 457, 821
- Orosz, J.A., Bailyn, C.D., 1995, *ApJ*, 446, L59
- Orosz J.A. & Hauschildt P.H., 2000, *A&A*, submitted
- Orosz, J.A. & Bailyn, C.B., 1997, *ApJ*, 477, 876 (OB97)
- Orosz, J.A., Remillard, R.A., Bailyn, C.D., & McClintock, J.E., 1997, *ApJ*, 478, L83
- Orosz, J.A., and Wade, R.A., 1999, *MNRAS*, 310, 773
- Press, W.H., and Rybicki, G.B., 1989, *ApJ*, 338, 277
- Roberts, D.H., Lehár, J., & Dreher, J.W., 1987, *AJ*, 93, 968
- Shahbaz T., 1998, *MNRAS*, 298, 153
- Shahbaz, T., Naylor, T., & Charles, P.A., 1994, *MNRAS*, 268, 756

- Shahbaz, T., Bandyopadhyay, R.M., & Charles, P.A., 1999a, *A&A*, 82, 346
- Shahbaz, T., van der Hooft, F., Casares, Charles, P.A., & van Paradijs, J., 1999b, *MNRAS*, 306, 89
- Shakura, N.I., and Sunyaev, R.A., 1973, *A&A*, 24, 337
- Stellingwerf, R.F., 1978, *ApJ*, 224, 953
- Stetson, P.B., 1987, *PASP*, 99, 191
- van der Hooft, F., Heemskerk, M.H.M., Alberts, F., & van Paradijs, J., 1998, *A&A*, 329, 538
- van Paradijs, J., and McClintock, J.E., 1995, in Lewin, W.H.G., van Paradijs, J., van den Heuvel, E.P.J., eds., *X-ray Binaries*. (Cambridge: Cambridge Univ. Press)
- Zhang, S. N., Harmon, B. A., Paciesas W. S., & Fishman, G. J., 1994, *IAU Circ.* 6209

Fig. 1.— Our  $BVIJK$  light curves folded on  $P_{orb} = 2.62191$  days. The open circles represent the high point which was removed from the data for analysis purposes. Optical magnitudes were found to be consistent with those of OB97. Overplotted are the best fit OH2000 models to the OB97 data set. This model required a partial eclipse by a disk with  $T_{outer} \approx 1000\text{K}$ . Note the poor fit in  $J$  and  $K$  due to the excess disk contribution in the infrared.

Fig. 2.— Our light curves (filled circles) are shown with the quiescent light curves of OB97 (filled triangles). Overplotted (lines) is the best fit model with no disk contribution. Below is shown a comparison stars of similar brightness (filled squares) to the program object and the residuals to the fit (filled circles). The scatter in the residuals matches that in the comparison stars, except near phase 0.5 in the  $B$  where the limb darkening effects are at a maximum.

Fig. 3.— Upper and lower limits to the size and temperature of a thin disk accretion flow. The thin lower line is  $T_{edge}$  which we argue represents a lower limit to the temperature of the outer disk due to illumination by the secondary star. The dashed vertical line represents the limit imposed by the lack of grazing eclipses due to an infinitely thin disk, at  $i = 70.2 \pm 1.9^\circ$  and  $Q = 2.6 \pm 0.3$ . This should be seen as an approximate limit due to its sensitivity to the chosen mass ratio and specific shape information. The upper curves represent the  $1\sigma$  (bold line) and  $3\sigma$  (dashed line) upper limits on spatial extent and temperature of a single temperature black-body disk which is assumed to contribute a constant flux dilution to the ellipsoidal light curves. The limits are derived from the  $V$  band data, which provided the most stringent limits on the allowed disk size and temperature.

Fig. 4.— Allowed region in  $Q - i$  space. Contours shown are the one and three  $\sigma$  limits imposed both by fits to the photometric data and by the constraint imposed by the measured  $v_{rot} \sin i$  of Israelian et al. (1999), as described in the text. The region above the dotted line would result in X-ray eclipses of the central source, which are not observed.

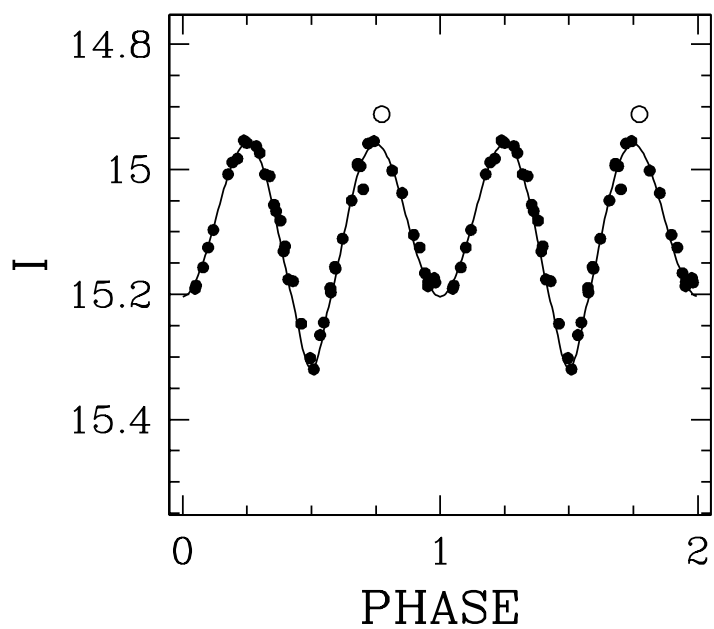
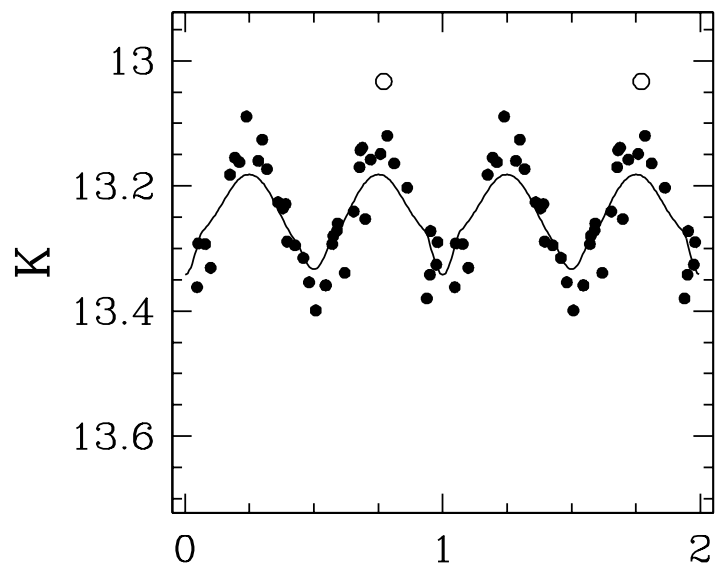
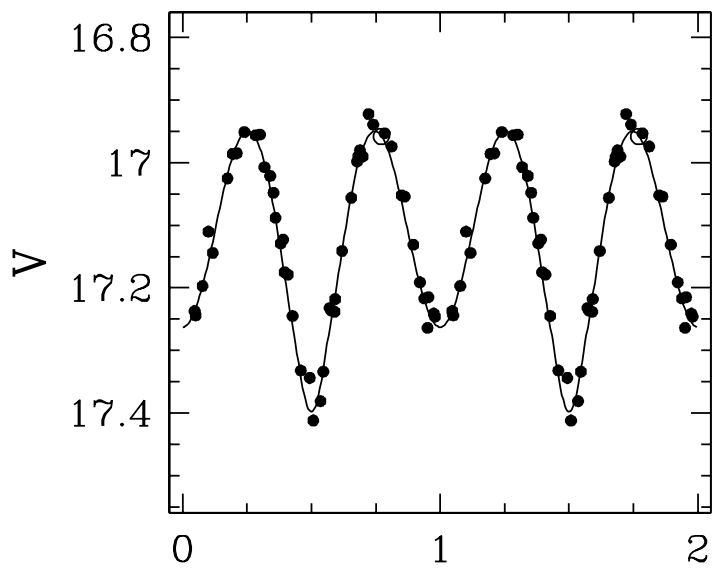
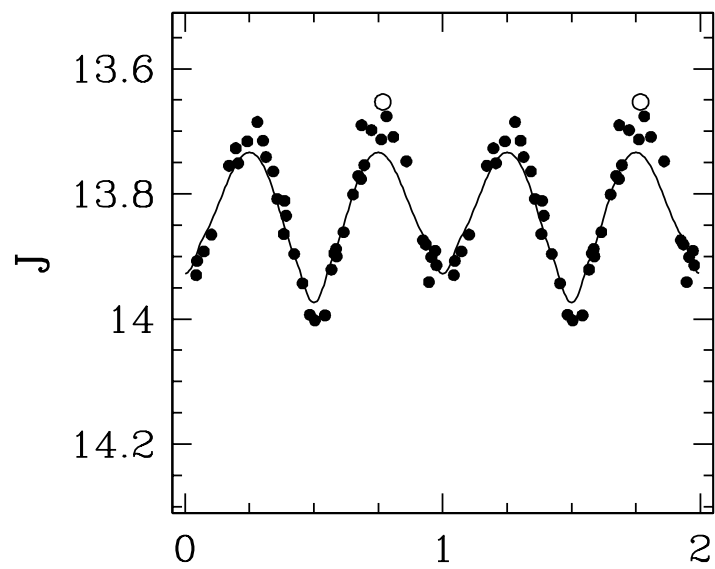
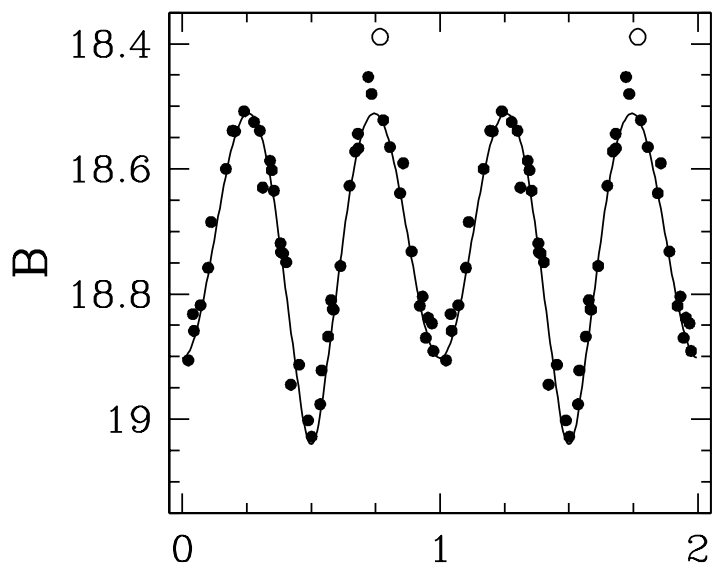
Fig. 5.— The probability distribution of  $M_1$ , found by weighting the values  $M_1$  derived over a range of  $Q$ ,  $i$ , and  $f(M)$  by an appropriate likelihood, as described in the text.

Table 1. Allowed Disk Dilution

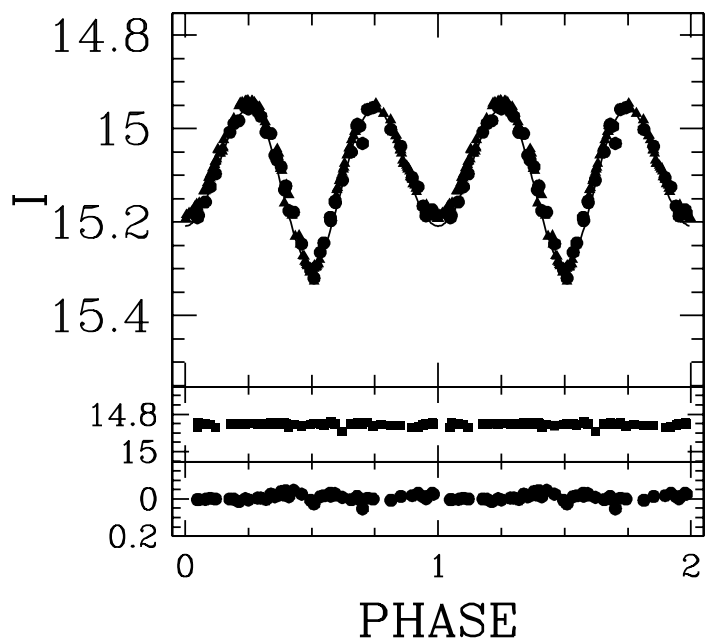
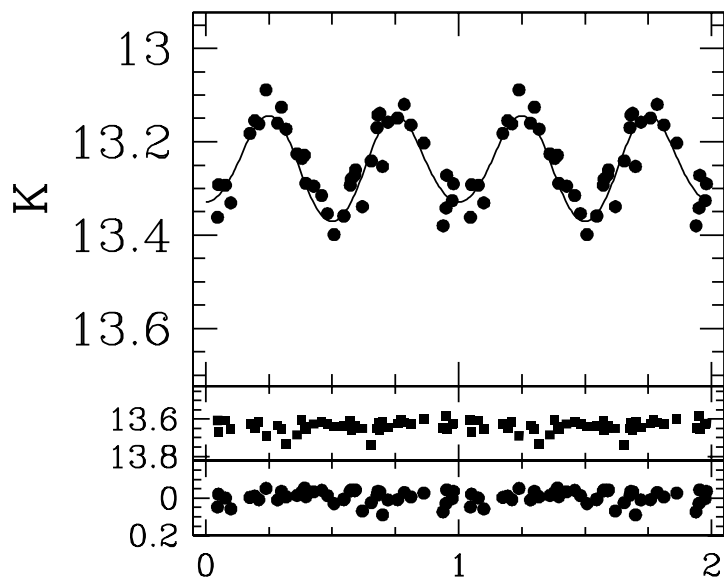
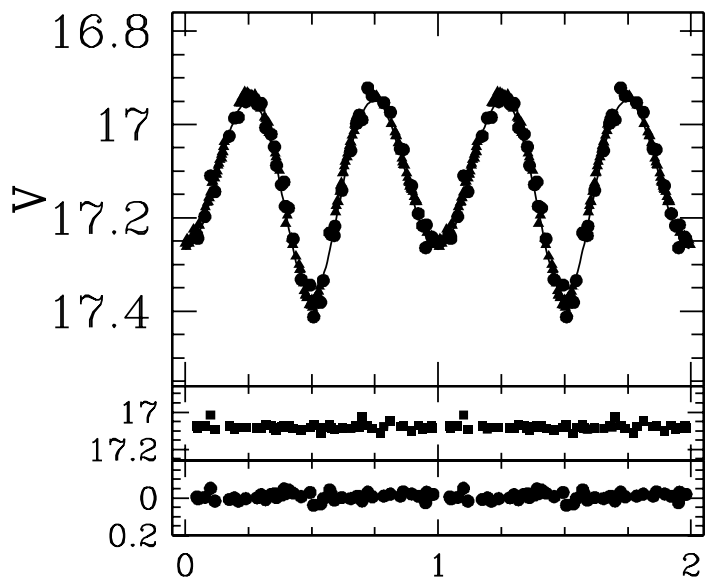
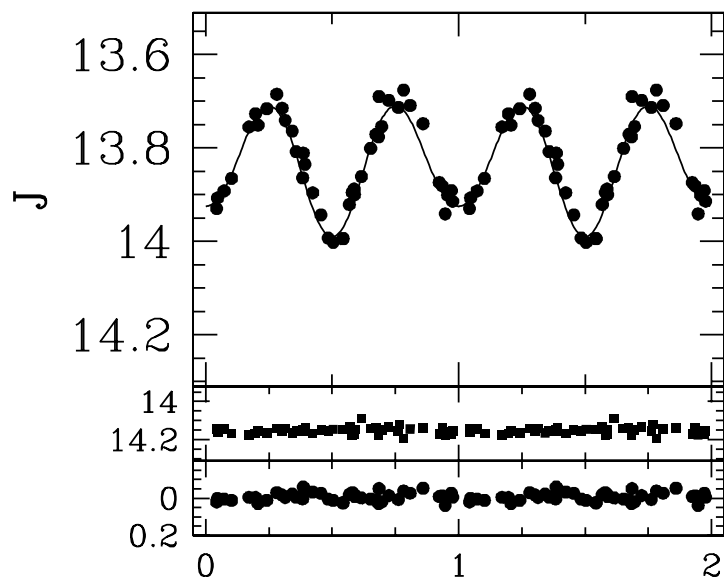
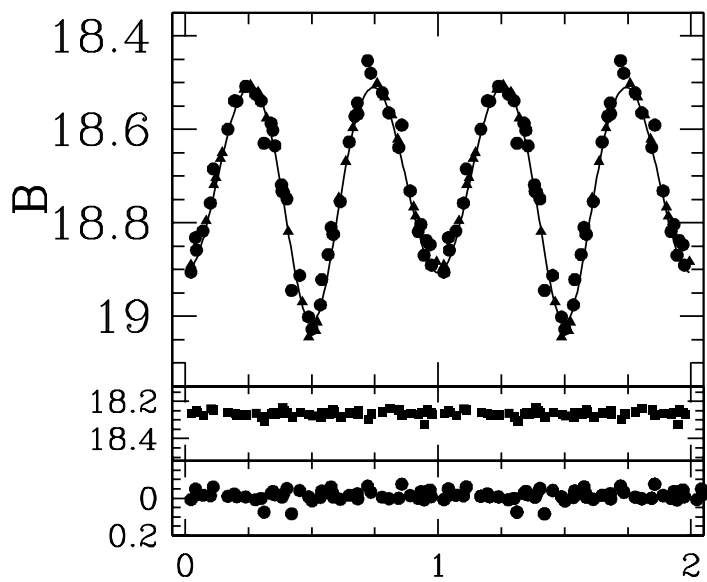
Filter	$1\sigma$	$3\sigma$
<i>B</i>	21%	28.5%
<i>V</i>	11.5%	17.5%
<i>I</i>	19.5%	25%
<i>J</i>	15%	24.5%
<i>K</i>	30%	46%

Table 2. Orbital Parameters of GRO J1655-40

Parameter	Result	Reference
Orbital Period, photometric (days)	$2.62191 \pm 0.0002$	This paper
$K_2$ ( $\text{km s}^{-1}$ )	$215.5 \pm 2.4$	Shahbaz et al. (1999b)
$v_{\text{rot}} \sin i$	$93.0 \pm 3.0$	Israelian et al. (1999)
Mass Function $f(M)/M_{\odot}$	$2.73 \pm 0.09$	Shahbaz et al. (1999b)
Q	$2.6 \pm 0.3$ (95% confidence)	This paper – see Fig. 4
Inclination $i$ (deg)	$70.2 \pm 1.9$ (95% confidence)	This paper – see Fig. 4
Primary Mass $M_1/M_{\odot}$	$6.3 \pm 0.5$ (95% confidence)	This paper – see Fig. 5
Secondary Mass $M_2/M_{\odot}$	$2.4 \pm 0.4$ (95% confidence)	This paper
Secondary Radius $R_2/R_{\odot}$	$5.0 \pm 0.3$ (95% confidence)	This paper



PHASE



PHASE

PHASE



